

# Analysis of Slope Stability Based on Four Machine Learning Models

## An Example of 188 Slopes

Menghan Zhang<sup>1</sup>, Jin Wei<sup>1\*</sup>

<sup>1</sup> School of Highway, Chang'an University, Xi'an 710064, China

\* Corresponding author, e-mail: [weijin@chd.edu.cn](mailto:weijin@chd.edu.cn)

Received: 08 June 2024, Accepted: 13 January 2025, Published online: 06 February 2025

### Abstract

To achieve rapid and precise prediction of slope stability, we propose an intelligent assessment method utilizing machine learning techniques. This approach aims to enhance the precision of slope stability evaluations, facilitating more effective and timely decision-making in geotechnical engineering. By analyzing 188 slope cases from domestic and international sources, we have identified six key feature variables to evaluate the Factor of Safety (FOS) for slope stability assessment. The dataset was established for evaluating slope stability, and to ensure robustness, it was divided into training and testing set using a 5-fold cross-validation approach. Four slope stability prediction models- GBM, SVM, XGB, and RF- were developed using machine learning algorithms. The accuracy of the models in predicting FOS for slopes was assessed using metrics such as MAE, MSE, RMSE, and  $R^2$ . The best-performing machine learning model, along with the finite element model developed using GeoStudio, was applied to engineering examples to compare their feasibility and efficiency. The research findings demonstrates that the GBM model has a minimal error between the predicted and actual slope FOS, highlighting its high accuracy. The model shows a strong correlation between predicted and actual FOS, indicating its superior performance relative to other models. GBM model and the finite element model align well with the actual field conditions. However, the GBM model stands out due to its higher accuracy and faster computational efficiency. Therefore, the GBM model offers a high degree of fit between the predicted FOS and the actual values, making it well-suited for evaluating slope stability.

### Keywords

factor of safety, machine learning, slope stability, finite element model

### 1 Introduction

Natural disasters occur frequently worldwide, and China is no exception. Due to its vast and geologically complex geology, China is particularly susceptible to such calamities. In 2022 alone, there were a staggering total of 5659 recorded geological disasters in the country, with 3919 instances of slope instability disasters. Consequently, several researchers [1, 2] have taken up studies on these cases of instability. The consequences of slope instability accidents can be devastating, causing significant harm to lives, properties and critical infrastructure. Notable examples include the Cher Tara Open Coal incident, the Chana Landslide [3], the Aniangzhai Landslide [4], the slope in Fa'er Town [5], the Baiyun Slide Complex [6] as well as various slopes in Fengjie County. Given this context, the evaluation of slope stability emerges as an immensely crucial research endeavor.

In recent decades, FOS is a parameter used to evaluate slope stability. Usually, the factors affecting slope safety are taken as the evaluation factors of slope safety factor. In recent decades, FOS has been widely used as a parameter to evaluate slope stability. Geometric parameters such as  $H$  and  $\beta$ , as well as strength parameters including internal  $\phi$  and  $c$ , play crucial roles in slope stability [7, 8]. Scholars have extensively researched and analyzed slope stability [9–12]. Various methods for determining the FOS include theoretical analysis, simulation tests, and numerical simulations [13]. The traditional limit equilibrium method, a type of theoretical analysis, assumes a predetermined critical slip surface and calculates resistance based on equilibrium equations [14]. However, in the implementation process of the traditional limit equilibrium method, the input

file is often manually modified according to different reduction coefficients, and the trial calculation is carried out continuously, making the process complex [15]. Numerical simulation methods such as finite difference and finite element are excellent techniques for addressing complex slope problems accurately and effectively. Nevertheless, these methods require modeling and analysis for each specific slope case, resulting in lengthy computational times [16]. Additionally, precise evaluation of boundary issues and replication of field environments pose challenges [17]. However, when facing diverse shapes, geological scenarios, and engineering conditions, the aforementioned methods have limitations in terms of calculation speed and accuracy. Therefore, there is a need for a method or technology that can overcome slow computation speeds and low accuracy while enabling quick determination of higher accuracy FOS and easy development [18]. Machine learning methods, renowned for their flexibility, efficiency, and accuracy, have been employed to automate slope assessment [19–21].

In recent years, the rapid advancement of machine learning methods has opened up new possibilities for studying highway slope stability. Machine learning (ML) methods can predict the FOS of a slope by considering various input parameters. Moreover, ML models can be customized based on the provided data, enhancing prediction accuracy. ML methods has emerged as one of the most reliable analysis methods for stability prediction [22, 23]. Notably, statistical techniques such as regression analysis within ML models establish relationships between dependent and independent variables, significantly contributing to accurate FOS predictions. Furthermore, various ML methods, including artificial neural networks and support vector machines [24] have demonstrated superior performance compared to regression analysis. To achieve better results, this study employs multiple sets of ML methods, such as Random Forest and Extreme Gradient Boosting (XGBoost) [25], which leverage ensemble learning to draw weighted conclusions from the decisions of numerous basic models.

Based on this background, the objective of this paper is to explore and evaluate the application of machine learning in predicting highway slope stability. Four ML models, namely Random Forest (RF), Support Vector Machine (SVM), XGBoost, and Gradient Boosting Machine (GBM) [26–32], will be employed to train and validate using existing 188 slope cases. By utilizing extensive input data and intricate models, machine learning enables the prediction of slope stability, thus improving accuracy and engineering efficiency. Evaluation indicators such as Mean Absolute Error (MAE), Mean Squared Error (MSE),

Root Mean Squared Error (RMSE) and R-squared ( $R^2$ ) will be utilized to assess model performance. A comparison with finite element analysis will also be conducted to evaluate the model's accuracy, efficiency, and practicality. Highway slopes are vital transportation infrastructure, connecting urban and rural areas. The stability of highway slopes has always been a critical factor influencing road safety and reliability [33–36], garnering attention from relevant departments [37, 38]. This paper aims to verify the applicability of the selected model in practical engineering by focusing on a loess highway slope example in Nanniwan Town, Yan'an City.

Through the development of this research, the paper aims to provide innovative ideas and methods for analyzing the stability of loess highway slopes. Additionally, it strives to offer more accurate, efficient, and reliable tools and guidance for the design and evaluation of highway engineering projects, particularly those related to slopes.

## 2 Data and methods

### 2.1 Data set and predictor variables

Slope stability analysis is a highly intricate problem, involving numerous interrelated factors. These factors can be classified into three main categories: slope configuration, geological and geotechnical properties of the rock and soil mass, and the influence of external loading conditions. Together, they provide a comprehensive assessment of the slope's behavior within the rock and soil mass under different loading scenarios. The significance of characteristic parameters on the slope's safety factor cannot be overstated. This study introduces a comprehensive set of characteristic parameters. Input parameters comprise slope height ( $H$ ), slope angle ( $\beta$ ), unit weight ( $\gamma$ ) of materials, cohesion ( $c$ ), internal friction angle ( $\varphi$ ), and pore water pressure ( $ru$ ). The slope safety factor ( $F$ ), serving as the output parameter, is utilized to determine the stability state of the slope.

To conduct a more compelling analysis, this study collected a total of 188 comprehensive slope cases. These cases encompassed both input parameters and output parameters, representing a wide range of stable and unstable slope states. This ensured that the dataset had excellent representativeness.

To evaluate the model's performance and determine the optimal approach for predicting slope safety factors, the dataset was divided into training and testing sets at a ratio of 3:1. Specifically, the testing set consisted of 47 slope cases, which were utilized to assess the model's effectiveness and to identify the most suitable model for predicting slope safety factors.

## 2.2 Data preprocessing

Data preprocessing holds paramount importance in ensuring the quality and integrity of subsequent data operations during model training. Its significance cannot be overstated, as it establishes a solid foundation for optimal data quality throughout the analysis pipeline. In this study, the completedData dataset underwent standardization using the "scale" function in RStudio software. This crucial preprocessing step ensures that the data across different columns are placed on the same scale, facilitating streamlined data analysis and processing in the subsequent stages.

During the data cleaning process, several steps were followed. Firstly, rows containing missing slope FOS values were deleted entirely from the dataset. Secondly, for rows with missing pore water pressure values, the mean imputation method was employed. This approach utilized the average value of pore water pressure due to the relatively small variation in these values.

In order to ensure data integrity, outliers with excessively high slope safety factor values were identified and removed based on rational judgment regarding plausibility. Lastly, considering that each slope case within the dataset is an independent entity and not time-dependent, duplicate entries of both input and output parameters were eliminated. This resulted in retaining only unique data records that represent distinct slope characteristics.

Through the application of the aforementioned data preprocessing steps, the integrity and consistency of the data have been successfully ensured. This meticulous process establishes a reliable foundation for subsequent model training and analysis.

## 2.3 Data visualization analysis

To conduct data visualization analysis, the "as\_tibble" function is utilized to convert a data frame into a tibble format. This format enhances the efficiency of subsequent data processing and analysis procedures. The "ggpairs" function is employed to generate a scatterplot matrix of the feature parameters, facilitating a rapid visual assessment of the relationships between variables.

Fig. 1 illustrates the scatterplot matrix of the feature parameters within the cleaned dataset, represented in the lower-left triangle. Each cell in the matrix represents a scatterplot depicting the relationship between two feature parameters. Furthermore, the diagonal section of Fig. 1 showcases density plots for each individual feature parameter, while the upper-right portion displays the correlation coefficients between pairs of feature parameters.

According to the upper-right portion of Fig. 1, it is evident that the correlation coefficient between FOS and  $\beta$  is  $-0.481$ , indicating a negative correlation and representing the strongest relationship among all variables. The correlation coefficient between  $C$  and  $\gamma$  is  $0.444$ , suggesting a positive correlation, albeit with a weaker association compared to FOS and  $\beta$ . Additionally, the correlation coefficient between  $\gamma$  and  $H$  is  $0.415$ , indicating a positive correlation. Generally, the correlations between other pairs of feature parameters exhibit moderate strengths.

Based on the correlation analysis of the feature parameters in this dataset, the highest absolute correlation value is  $0.481$ , signifying that there is no significant redundancy among the data. Therefore, each feature parameter plays an essential role in predicting FOS.

To summarize, the distribution of feature parameters within the dataset demonstrates no redundant information, and all parameters exhibit reasonable distributions. This suggests that the dataset is of good quality, providing a reliable foundation for subsequent model training and analysis.

## 2.4 Machine learning methods

### 2.4.1 Gradient Boosting Machine

GBM is a boosting tree model based on the gradient descent algorithm. It leverages the collective strength of multiple weak learners to construct a powerful predictive model, commonly used for regression problems. Each weak learner in GBM focuses on optimizing and adjusting the prediction errors made by the preceding weak learners. This iterative process allows GBM to effectively capture the complex relationships and nonlinear features present within the data.

By continuously improving its predictive performance through iterations, GBM enhances the accuracy and robustness of the model. It combines the predictions from multiple weak learners, gradually refining its understanding of the data and achieving superior predictive results.

### 2.4.2 Support Vector Machine

The SVM regression model aims to find an optimal hyperplane that fits the data, as illustrated in Fig. 2. This hyperplane is designed to maximize the margin between the sample points and the fitting line while ensuring that the error estimation remains within a specified range.

To handle nonlinear data distributions, the SVM regression model employs a kernel function that maps the features into a higher-dimensional space. This transformation enables the model to effectively capture complex relationships between variables.

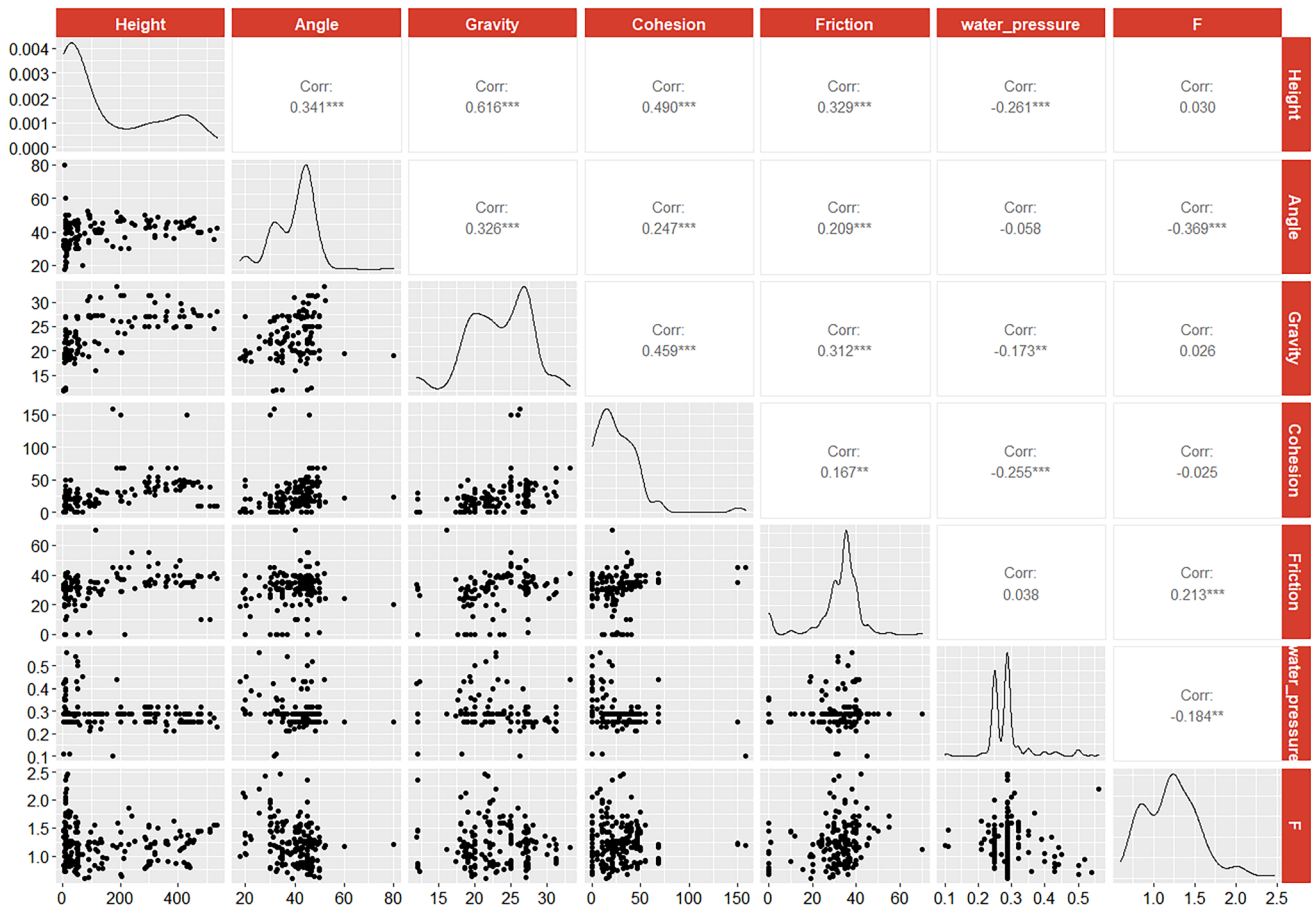


Fig. 1 Correlation matrix plot of the feature parameters

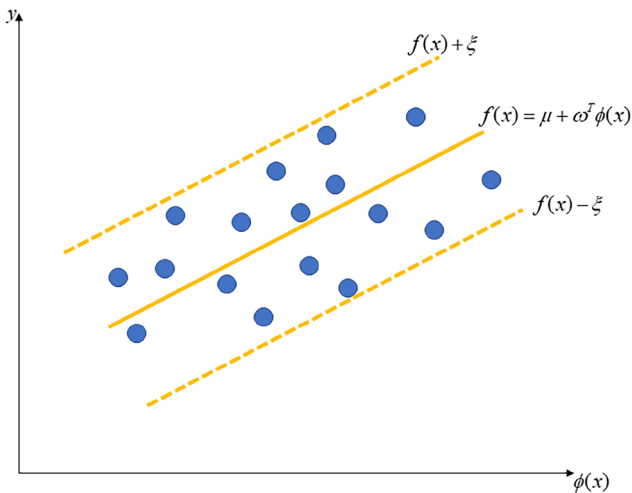


Fig. 2 Illustration of the SVM regression algorithm

The SVM regression model is renowned for its ability to handle intricate data distributions and deliver precise regression results.

### 2.4.3 Random Forests

Fig. 3 illustrates a RF, which is an ensemble learning algorithm consisting of multiple decision trees. Each decision

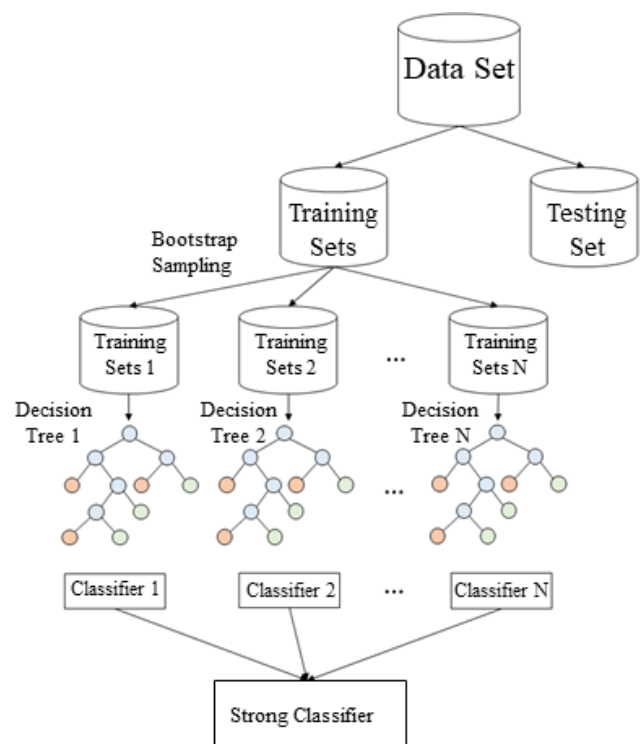


Fig. 3 Illustration of the random forest algorithm for classification and regression tasks

tree within the random forest operates independently from the others. In the regression model for slope safety factors, each individual regression decision tree predicts the safety factor for a specific slope.

To obtain the final prediction of the FOS, the predictions from all the decision trees are averaged. This aggregation process ensures that the collective wisdom of the decision trees is utilized to generate a more accurate and robust prediction.

In the training set of slopes, the RF algorithm selects a subset of features at each node of the tree for branching and growth. This ensures that every feature undergoes the branching and growth procedure within the trees.

Specifically, during the growth process, a subset of  $m$  features (where  $m$  is less than the total number of available features) is selected. The selection of these features follows the principle of minimizing node impurity, where the most informative feature is chosen for branching. It is important to note that the value of  $m$  remains constant throughout the entire growth process of the RF.

#### 2.4.4 Extreme Gradient Boosting

XGBoost is a powerful ensemble learning method, similar to RF, that combines multiple weak learners. It is represented as a boosting tree model, as illustrated in Fig. 4. However, unlike RF, in the XGBoost model, each weak learner is interdependent, meaning that the input samples of previous regression trees influence the training and prediction results of subsequent regression trees.

In a regression model, the final prediction value of the FOS is obtained by summing the scores of fitting residuals from all decision trees. The objective function of XGBoost consists of two components: the loss function and the regularization term. The loss function measures the extent to which the regression model accurately fits the data, and it is continuously trained to compensate for any gaps

or inconsistencies within the trees. By combining multiple trees, the model aims to simulate the true distribution of the data. On the other hand, the regularization term is employed to control the complexity of the model and prevent overfitting.

#### 2.4.5 The Finite Element Theory

The GeoStudio software is widely used in geotechnical engineering to simulate various aspects, including parameter uncertainty, slope risk analysis, and reliability calculations. The software employs the limit equilibrium method, which takes into account the Mohr-Coulomb strength criterion and static equilibrium conditions.

This approach involves dividing the slope into soil slices and assessing its stability by analyzing the forces of sliding and resistance to sliding. The analysis is based on the principles of the Mohr-Coulomb theory, and the Morgenstern-Price method is utilized to establish the model. By selecting appropriate shear strength parameters, pore water pressure models, and considering the geometric dimensions and internal characteristics of the slope, accurate determination of the FOS can be achieved.

### 3 Model establishment and parameter tuning

#### 3.1 Model establishment

The FOS serves as a reliable predictor for assessing the stability of highway soil slopes. However, the precision of different machine learning regression models may vary. Therefore, this section focuses on researching and comparing the performance of various machine learning models in predicting FOS.

As illustrated in Fig. 5, GBM, RF, SVM, and XGB models are employed to evaluate their predictive accuracy for FOS. The objective is to identify the optimal model that yields the most accurate predictions for FOS.

#### 3.2 Model evaluation

In the FOS regression algorithm, the accuracy of the regression model is evaluated through two aspects. Firstly, the magnitude of the error between the predicted FOS and the actual FOS is used as a measure of the model's performance. Secondly, the fit between the predicted FOS and the actual FOS is assessed to evaluate the model's performance.

Several metrics, including MAE, MSE, RMSE, and  $R^2$  are employed to gauge the accuracy and precision of the model in predicting FOS.

1. MAE specifically measures the magnitude of the error between the predicted FOS and the actual FOS.

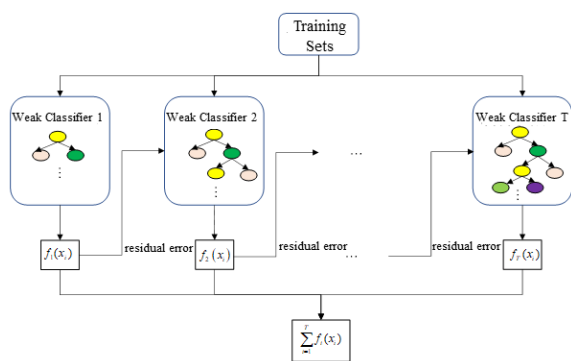


Fig. 4 Conceptual diagram of XGBoost algorithm for regression classification

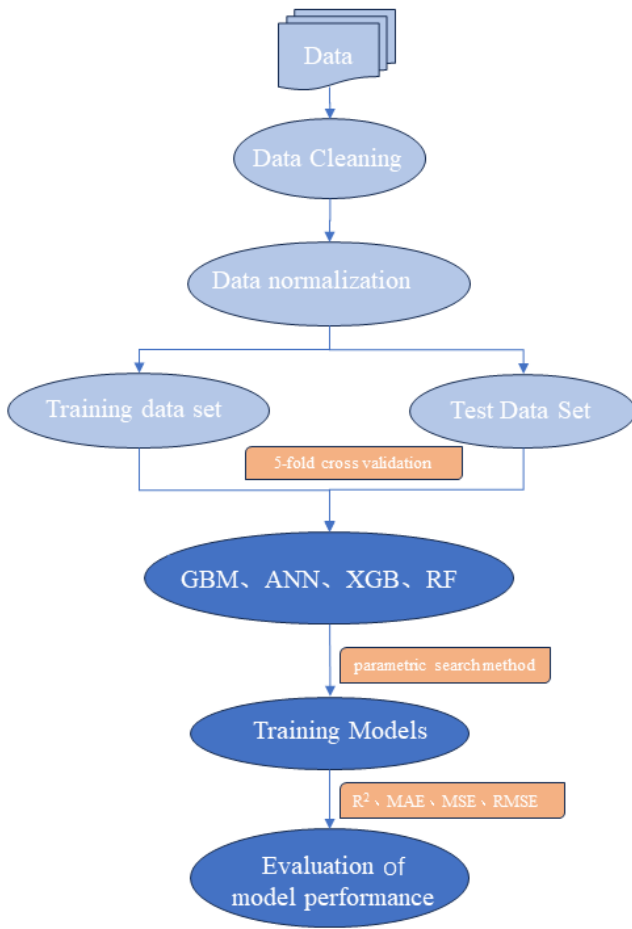


Fig. 5 Machine learning flowchart

The calculation formula for MAE is as follows:

$$MAE = \frac{1}{n} \sum_{i=1}^n |\hat{y}_i - y_i| \quad (1)$$

- MSE reflects the deviation between the predicted FOS and the actual FOS. A value closer to 0 indicates higher accuracy of the model. The calculation formula for MSE is as follows:

$$MSE = \frac{1}{n} \sum_{i=1}^n (y_i - \hat{y}_i)^2 \quad (2)$$

- RMSE is the square root of the MSE metric, representing the sample standard deviation of the difference between the actual slope safety factor and the predicted FOS.

$$RMSE = \sqrt{\frac{1}{n} \sum_{i=1}^n (y_i - \hat{y}_i)^2} \quad (3)$$

- The patterns captured by the model from the data can be measured by  $R^2$ .  $R^2$  reflects the model's goodness of fit, with values typically ranging from 0 to 1.

A value closer to 1 indicates a higher degree of fit between the model's predictions and the true FOS.

$$R^2 = 1 - \frac{\sum_{i=1}^n (y_i - \hat{y}_i)^2}{\sum_{i=1}^n (y_i - \bar{y}_i)^2} \quad (4)$$

In Eq. (4),  $n$  represents the number of slopes,  $y_i$  denotes the true FOS of the  $i$ -th sample, and  $\hat{y}_i$  represents the predicted FOS of the  $i$ -th sample.

### 3.3 Model establishment

Before proceeding with modeling, the *makeRegrTask* function is employed to prepare the model for a regression task. The data parameter is used to store the dataset, while the target parameter specifically designates the FOS as the response variable. Subsequently, proceed to model using the SVM, XGB, RF, and GBM algorithms.

The *Caret* package is an essential tool for various aspects of predictive modeling, including data partitioning, preprocessing, feature selection, model tuning, and assessment of variable importance. Within the *Caret* package, the *createDataPartition* function can be utilized to effectively divide the dataset into two distinct parts: one for model training and the other for model testing. This partitioning process enables the evaluation of the model's performance and its ability to generalize well beyond the training data. In the testing and training sets, the following independent variables are defined:  $\gamma$  as  $x_1$ ,  $C$  as  $x_2$ ,  $\phi$  as  $x_3$ ,  $\beta$  as  $x_4$ ,  $H$  as  $x_5$ , and  $ru$  as  $x_6$ . Additionally, the FOS is defined as the response variable  $y$ .

To address the model's sensitivity to sample selection within a specific dataset, 5-fold cross-validation is employed. This technique divides the dataset into multiple distinct subsets, as depicted in Fig. 6. The model is then

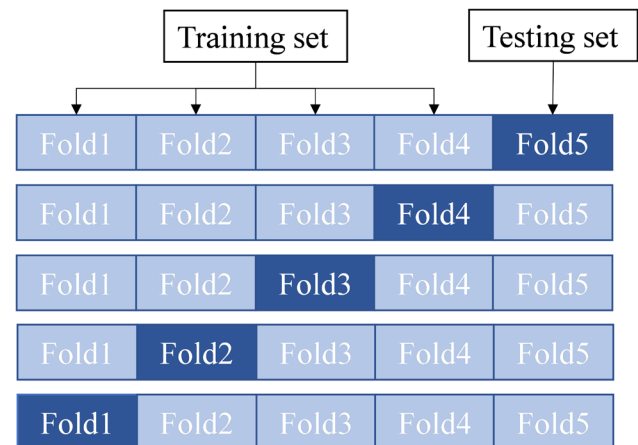


Fig. 6 Schematic of 5-fold cross-validation

trained and tested using each subset individually. During each iteration, one subset serves as the testing set, while the remaining subsets are used for training.

By utilizing this approach, the variance of performance estimates can be reduced. The model's performance is evaluated on each subset, considering metrics such as  $R^2$ , MSE, RMSE, and MAE. To obtain a more robust estimate of the model's generalization performance, the average of these five performance values is calculated. This comprehensive evaluation allows for a thorough assessment of the model's performance and its ability to generalize beyond the training data.

To optimize hyperparameters and achieve optimal model performance, *GridSearch* is employed. This technique systematically searches the predefined hyperparameter space to identify the best combination.

Subsequently, 5-fold cross-validation is utilized to comprehensively evaluate each potential hyperparameter combination on the training data. This process ensures a thorough assessment of the model's performance across different hyperparameter settings.

Ultimately, the hyperparameter combination that yields the best performance on the validation data is selected as the final model. The evaluation metric used for this selection process is  $R^2$ , which assesses the model's ability to capture the variance in the target variable.

### 3.3.1 Fine-tuning of GBM regression model Parameters

The GBM regression model utilizes the *trainControl* function to automate parameter tuning. This function specifies the cross-validation method and parameter search approach employed during model training. In this study, 5-fold cross-validation and *GridSearch* are utilized to optimize the model's hyperparameters and maximize performance metrics.

After conducting multiple iterations, the hyperparameter ranges for the GBM regression model have been established and are presented in Table 1. These ranges were utilized in conjunction with cross-validation and other processes to fine-tune the hyperparameters of the GBM model.

By evaluating the model's performance using each combination of hyperparameters, the  $R^2$  value for the

model with the selected parameter combination on the dataset is illustrated in Fig. 7. This analysis enables the identification of the combination that yields the best performance on the dataset.

Based on the optimal  $R^2$  value obtained, the model's optimal parameter combination can be determined as follows:  $n.trees = 120$ ,  $interaction.depth = 3$ ,  $shrinkage = 0.13$ , and  $n.minobsinnode = 3$ .

### 3.3.2 Optimization of parameters for other regression models

After multiple rounds of parameter tuning, the optimal parameter combinations for each model have been determined, as shown in Table 2. The XGB, RF, and SVM models have been optimized based on different hyperparameters.

## 4 Result

### 4.1 Evaluation of machine learning model results

Table 3 presents the performance evaluation of the four models, including  $R^2$ , MAE, MSE, and RMSE. Through comparative analysis, it is observed that the GBM regression model exhibits the highest  $R^2$  value, indicating the best fit to the data. Additionally, it demonstrates the smallest RMSE, MSE, and MAE values among the four machine learning models, signifying the smallest errors.

Based on these evaluation metrics, it can be concluded that the GBM regression model achieves the highest accuracy among the models considered.

As shown in Table 4, the GBM regression model exhibits absolute errors in the test samples, representing the disparities between the predicted values and the actual values. The majority of these absolute errors are less than 0.1, indicating minimal deviations between the predicted and true FOS.

Moreover, the relative error, calculated as the absolute error divided by the true value, approaches nearly zero in absolute value. This suggests that the GBM regression model achieves a high level of accuracy, with very small disparities between the predicted and true values.

Fig. 8 presents a scatter plot generated using the *ggplot* function in the R programming language. This plot showcases a two-dimensional density representation. In the scatter plot, each data point represents a test data point. The x-coordinate corresponds to the true values, while the y-coordinate represents the predicted values of the GBM regression model.

The scatter plot indicates that the predicted values align closely with the diagonal line. The solid blue line, representing the fitting line, closely follows the diagonal

**Table 1** Adjusted hyperparameter ranges for GBM regression model configuration

Parameter	Parameter Ranges
<i>n.trees</i>	c (120, 140, 150,160)
<i>interaction.depth</i>	c (1, 2, 3, 4)
<i>shrinkage</i>	c (0.1, 0.11, 0.12, 0.13, 0.14)
<i>n.minobsinnode</i>	c (2, 3, 4, 5, 6, 7)

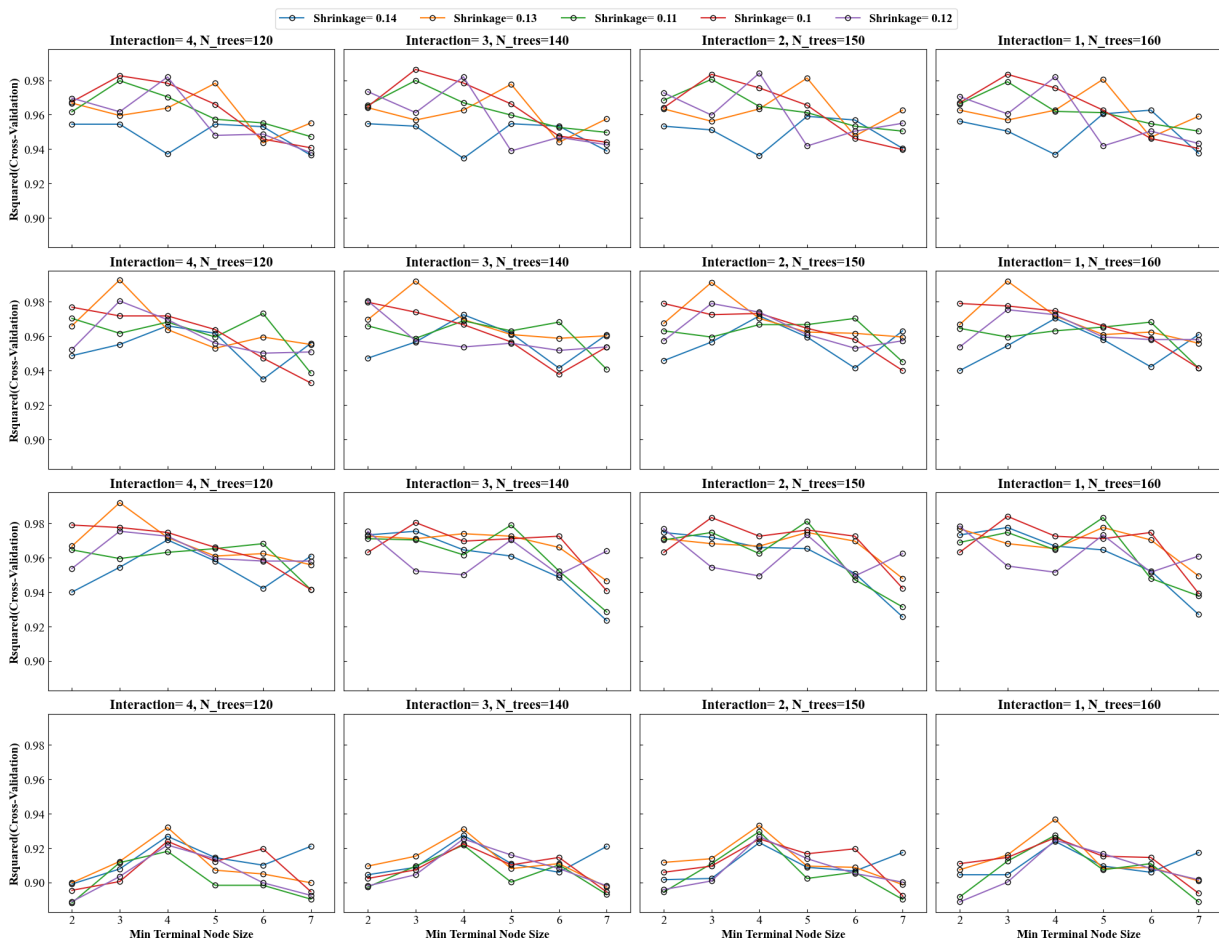


Fig. 7 R<sup>2</sup> for different parameter combinations of GBM model with adjusted hyperparameter ranges

Table 2 Optimal parameter combinations for four machine learning models after parameter tuning

Models	Best parameter combination
GBM	<i>n.trees</i> = 120, <i>interaction.depth</i> = 3, <i>shrinkage</i> = 0.13 and <i>n.minobsinnode</i> = 3
RF	<i>mtry</i> = 4
XGB	<i>nrounds</i> = 40, <i>lambda</i> = 0.001, <i>alpha</i> = 0.2 and <i>eta</i> = 1e-04
SVM	<i>sigma</i> = 0.09 and <i>C</i> = 30

Table 3 Comparative analysis of evaluation results for each model

Model → indicator ↓	GBM	XGB	RF	SVM
MAE	0.069154	0.111443	0.102410	0.127840
MSE	0.007334	0.021562	0.013593	0.025044
RMSE	0.085641	0.146842	0.116588	0.1582547
R-squared	0.989369	0.967642	0.981570	0.9643483

line. This suggests that the predicted values have minimal errors compared to the true values.

The scatter points fall within the region between the two dashed lines, indicating that the errors between the

Table 4 A comparison of the FOS and the predicted values for selected samples in the test set by the GBM regression model

	The predicted value of GBM regression model	True value	Absolute errors	Relative errors
1	2.021	1.945	0.076	0.0390746
2	1.294	1.360	-0.066	-0.0485294
3	1.000	0.933	0.067	0.0718114
4	0.813	0.785	0.028	0.0356688
5	0.580	0.496	0.084	0.1693548
6	0.800	0.722	0.078	0.1080332
7	1.662	1.771	-0.109	-0.0615471
8	1.569	1.634	-0.065	-0.0397797

predicted and true values are within an acceptable range. Furthermore, when the scatter points are closer to the diagonal line, it signifies smaller errors and higher accuracy in the predictions. Overall, based on this analysis, the GBM regression model demonstrates a high degree of fit.

Fig. 9 displays scatter plots mapping the absolute error distribution across four distinct regression models. The z-axis

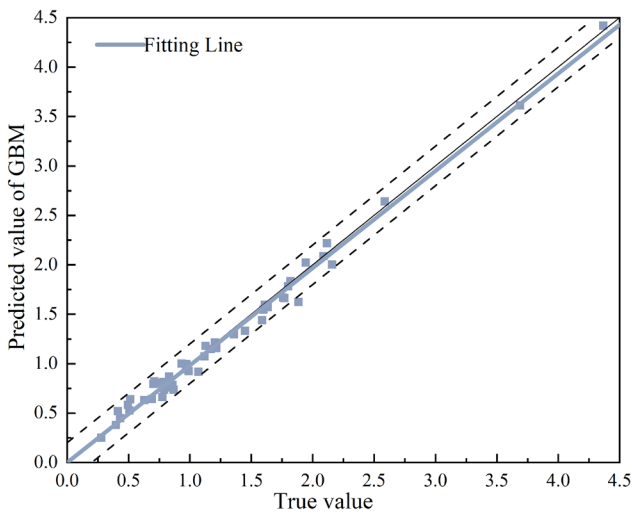


Fig. 8 True values and predicted values of the GBM regression model

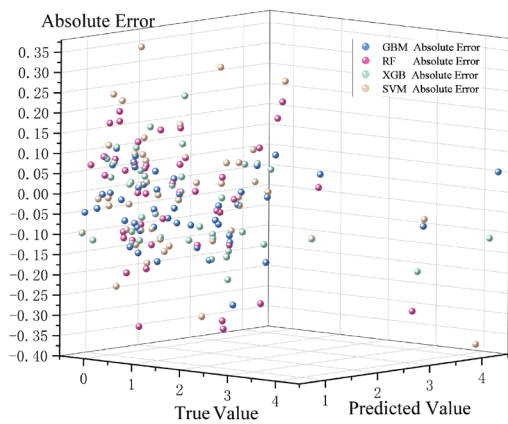


Fig. 9 Scatter plot of the absolute error distribution in the regression model

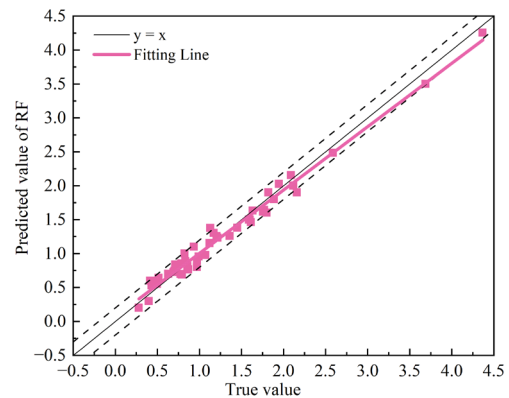
quantifies error magnitude, while the x-axis and y-axis correspond to true and predicted model values, respectively. Represented in blue, the spheres demarcate errors associated with the GBM regression model, with pink spheres denoting errors for the RF regression model, green for the XGB regression model, and yellow for the SVM regression model.

A spatial analysis of the sphere distribution reveals that the pink and yellow spheres are dispersed over a wider range, signifying larger discrepancies in the predicted outcomes of their respective models. In contrast, the blue spheres, representing the GBM model, exhibit a more concentrated formation. The latter are chiefly arrayed near the plane of zero error, underscoring a minimal deviation between the predicted and true values.

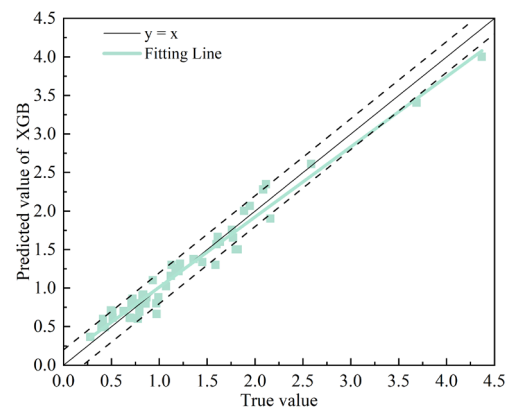
The comparative assessment hence suggests that the GBM regression model outperforms the others in precision, as indicated by its reduced absolute error. This model

demonstrates higher accuracy in producing predictions that closely align with the true values, a critical metric in the fidelity of regression models within the domain of civil engineering.

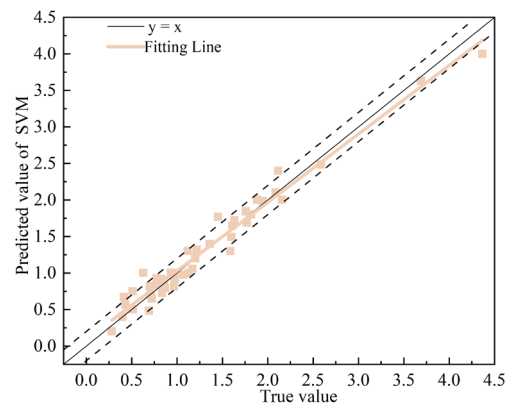
Fig. 10 displays a scatter plot with three different data series representing the RF, XGB, and SVM regression models. The x-axis represents the true values, while the y-axis represents the corresponding predicted values. Each



(a)



(b)



(c)

Fig. 10 Scatter plot of the true values and predicted values for the (a) RF, (b) XGB and (c) SVM regression models

data point in the plot represents an individual observation or data point from the dataset. The scatter plot allows us to visualize the relationship between the true values and the predicted values for each regression model.

The Residual Cumulative Distribution Plot is a commonly employed tool in regression models for evaluating the statistical fit's quality. It offers valuable insights into the distribution of residuals, unveiling potential patterns or trends within their distribution. This plot presents the cumulative distribution of residuals, enabling us to analyze their distribution and proportions effectively. Therefore, it serves as a useful means of assessing the overall goodness-of-fit of the regression model.

In Fig. 11, the residual cumulative distribution lines of the RF, GBM, XGB, and SVM regression models are represented by the colors red, blue, green, and orange, respectively. The GBM regression model's residual line is positioned below the other lines, indicating that a majority of its residuals are relatively small. The XGB and RF regression models show similar patterns in their residual lines. Hence, there is no significant difference in performance between the XGB and RF regression models, as their cumulative distribution lines are close to each other but positioned above the GBM line. On the contrary, the SVM regression model exhibits higher residuals for most of its samples compared to the other models. Therefore, the SVM regression model performs less favorably than the other models. Consequently, it can be concluded that the GBM regression model demonstrates the best fitting performance, while the SVM regression model exhibits the poorest fitting performance.

Fig. 12 depicts the boxplots representing the GBM, RF, XGB, and SVM regression models based on the evaluation metric RMSE. Among these models, the GBM regression model exhibits the smallest mean value when evaluated

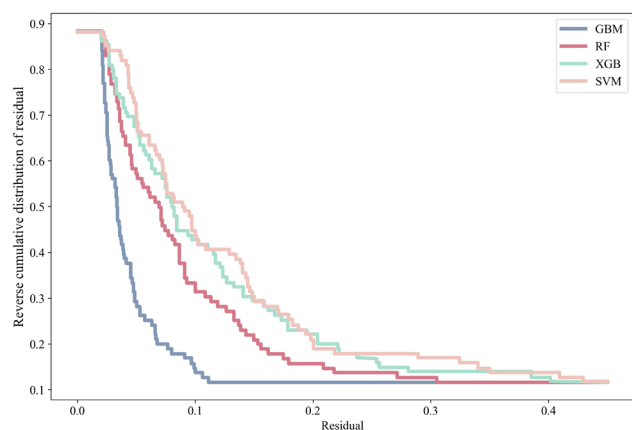


Fig. 11 Residual cumulative distribution plot

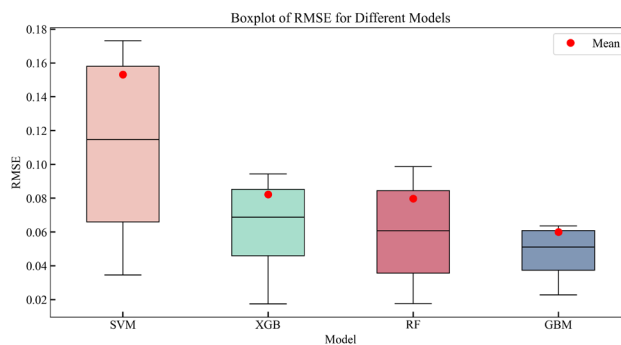
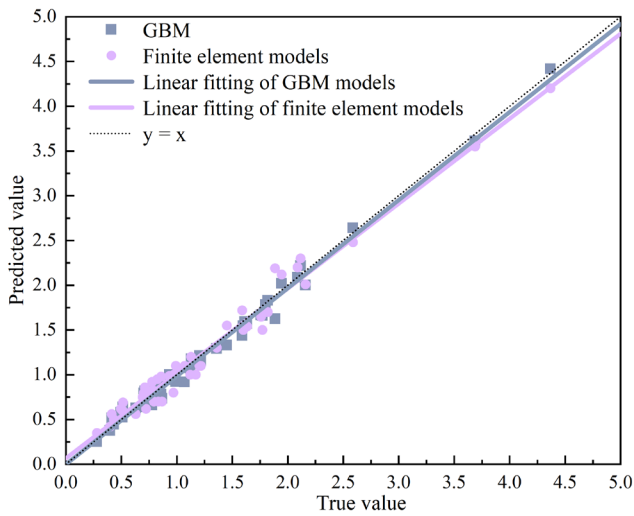


Fig. 12 Boxplot of the RMSE performance evaluation metric for different models

using the RMSE metric. The black solid line within each boxplot denotes the minimum value on the left side and the maximum value on the right side for each model. Notably, the SVM model displays a substantial difference between its maximum and minimum values, indicating significant variation compared to the other three models. Conversely, the lengths of the black solid lines for the GBM, RF, and XGB regression models are similar, suggesting a comparable range between their maximum and minimum values. In conclusion, the GBM regression model demonstrates superior performance, while the RF and XGB regression models exhibit similar levels of performance, and the SVM regression model performs the least effectively.

#### 4.2 Comparison between Machine Learning Methods and Finite Element Analysis

In the previous section, it was determined that the GBM regression model achieved the highest accuracy in predicting the FOS. Building upon this finding, our focus now shifts towards comparing the results of the limit equilibrium method's simulation with the predictions of the GBM regression model. The ultimate objective is to identify the most accurate model for FOS prediction by evaluating both the finite element analysis method and the machine learning method. This article primarily utilizes the SLOPE/W module within the GeoStudio software, which serves as a powerful tool specifically designed for analyzing slope stability. The SLOPE/W module employs the limit equilibrium theory to model and analyze the stability of slopes characterized by various soil types and intricate stratigraphy. Moreover, it takes into consideration the pore water pressure conditions prevalent within the slopes. Comparisons of the modeled safety factors are presented in Fig. 13, depicting the comparisons between the GBM regression model and the finite element analysis method. The x-axis represents the true values, while



**Fig. 13** Comparison between the predicted values and true values of the FOS using the GBM and finite element analysis model

the y-axis represents the predicted safety factors by the GBM model and those obtained through the finite element analysis method. A more accurate prediction is indicated by points closer to the diagonal line. As observed, the distribution of points representing the predicted values by the GBM regression model is closer to the diagonal line, whereas the points representing the finite element model exhibit relatively greater dispersion. Consequently, the finite element analysis method performs slightly inferior compared to the GBM regression model in terms of predicting the FOS when compared to the true values.

Fig. 14 present the errors between the predicted values and true values for the corresponding GBM regression

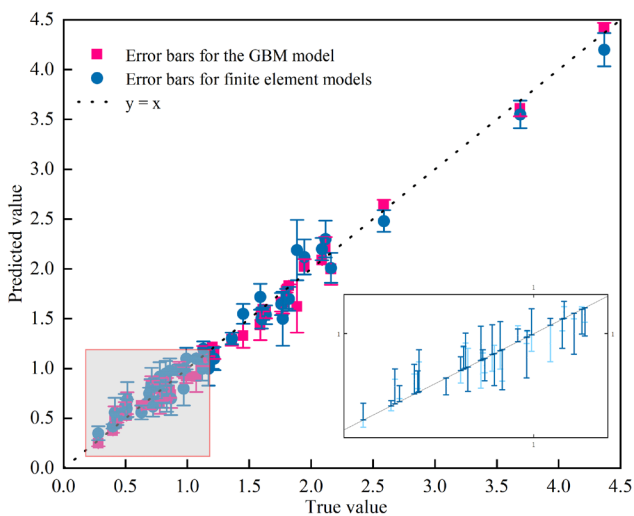


**Fig. 14** Error bar plot depicting the difference between the predicted values and true values of the FOS by GBM regression model and finite element model

model and finite element analysis, respectively. The length of the error bars reflects the magnitude of the differences between the predicted and true values, with longer error bars indicating larger disparities.

Through careful comparison and analysis of these two plots, it becomes apparent that the errors in the FOS values calculated by the finite element model are notably larger within the range of 2 to 2.5 when compared to the range of 0 to 1.5. Furthermore, the errors in the predictions made by the finite element model are generally greater than those in the GBM regression model. This is evident from the overall shorter error bars in the GBM regression model for most data points.

Based on this analysis, it can be concluded that the GBM regression model provides more accurate predictions of the slope's FOS. The results indicate that using the GBM regression model yields smaller errors and therefore represents a more reliable approach for predicting the FOS.

It is important to note that when considering time efficiency, constructing the proposed finite element model necessitates the individual construction of geometric conditions, definition of the analysis method, and specification of internal characteristics for each slope case. Once the model is established for each case, the FOS can be calculated in batches. However, this modeling process involves creating different slope dimensions and internal features, which would typically require approximately 9 hours for the 47 slope cases mentioned in this article.

Please bear in mind that the provided time estimation is based on the available information and may vary depending on factors such as the complexity of the slope cases, computational resources, and modeling techniques utilized.

In contrast, machine learning models provide the advantage of predicting FOS by inputting a dataset of relevant slope feature parameters into the model. This approach offers faster computation times compared to the finite element modeling process. During training, parameter grid tuning and 500 000 iterations are performed, taking only 2 minutes.

In summary, the use of machine learning models not only provides higher accuracy but also significantly reduces computation time. This demonstrates the effectiveness of the proposed method outlined in this article.

Please note that the provided information is based on the details given. Actual performance and speed may vary depending on factors such as the size and complexity of the dataset, computational resources, and specific implementation techniques.

### 4.3 Engineering application examples

The proposed project is situated in the southwestern part of Baota District, Yan'an City. Its construction is expected to have a positive impact on enhancing the efficiency of the transportation system in the Nan Ni Wan Scenic Area. The project's starting point is located in Mafang Village, Nan Ni Wan Town, with a connection to the existing S303 road. From there, it proceeds westward along the planned S303 transit line, passing through Taoshuwan Gully until it reaches Wangzhuang. After traversing a tunnel and connecting with the existing old road, the route continues through Nan Panlong and Miaotai, following the alignment of the Junwei Gully. To traverse the area, the route incorporates nine mountain ridges through tunnels while remaining aligned with the Junwei Gully. It then passes through Rentai and Yejiashuang before crossing under the disused West Extension Railway, Bao Mao Expressway, and the operational West Extension Railway double track. Finally, the route intersects with G210 at San Shili Pu. The total length of the route is 32.022 kilometers.

The research object focuses on the slope of the Fanzhuang Road segment, specifically from K12+130 to K12+350. This slope is situated near Fanzhuang Village, Nan Ni Wan Town, at the exit of the Nan Panlong Tunnel. Serving as a road embankment slope, it has a height of approximately 45 meters and is constructed using a stepped cutting method. It consists of a total of nine steps, each measuring 5 meters in height. The third and fifth steps have a width of 5 meters, while the remaining steps have a width of 3 meters.

Based on the investigation conducted, it has been determined that the slopes in this area possess loose soil structure with significant pore development. Consequently, after excavation of the road embankment slopes, instability may occur due to the influence of upper loading and heavy rainfall.

As discussed in Section 4.2, it is established that the GBM regression model offers the most accurate predictions for the FOS of slopes. Building upon this finding, this section focuses on the development of a prediction model for the FOS of highway soil slopes based on the GBM regression model. The slope's characteristic parameters obtained from geotechnical tests are presented in Table 5. Utilizing these slope characteristic parameters as independent variables, a predicted FOS value of 1.498 is derived.

The slope of Nan Ni Wan is chosen as the research object, and the VADOSE/W module is employed to establish the

model. By inputting the slope characteristic parameters obtained from Table 5, the FOS of the slope is calculated using the Mohr-Coulomb model. Fig. 15 illustrates the model representing a slope with a height of 68 m on the left side and 24 m on the right side. The base width measures 120 m, while the top width is 20 m. Moreover, the slope consists of nine stepped sections, each with a height of 5 m. In Fig. 15, the green portion represents the most critical sliding surface of the slope, indicating that the slope failure occurs due to sliding from left to right. Through numerical simulations, it has been determined that the most critical sliding surface of this slope lies between the first and sixth steps, with a calculated FOS of 1.524. This suggests that the slope is considered stable. Additionally, during a field survey, cracks were observed in the third step. Consequently, the numerical results align with the actual conditions and are consistent with the predictions made by the GBM model.

### 5 Conclusions

Based on the slope characteristic parameters and the FOS, a relationship has been established where the slope characteristic parameters act as independent variables and the FOS serves as the response variable. In this study, machine learning methods, including GBM, SVM, XGB, and RF models, are proposed for predicting the FOS. These models are compared with the finite element model to identify the most accurate method for predicting the FOS. The feasibility of the proposed models is then validated using slope engineering examples, leading to the following conclusions:

1. Utilizing the GBM, SVM, XGB, and RF models, we establish a predictive regression model for FOS and compare their performance. Among these models, the GBM regression model outperforms the others, achieving an MAE of 0.069154, MSE of 0.007334, RMSE of 0.085641, and R2 of 0.98937. Hence, it

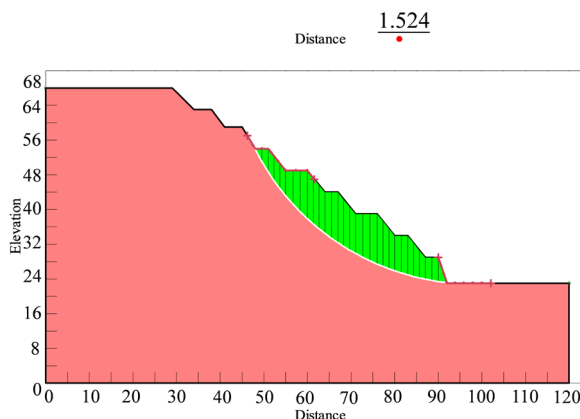


Fig. 15 Calculation results graph of the slope model

Table 5 Slope characteristic parameters

H/m	$\beta/^\circ$	ru	C/kPa	$\gamma/\text{kN/m}$	$\phi/^\circ$
45	32	0.15	50	20.5	28.7

can be concluded that the GBM regression model is well-suited for accurately predicting the FOS.

2. By using the feature parameters from the slope cases in the test set as independent variables, we model and perform finite element analysis for FOS in GeoStudio. When comparing the finite element model with the GBM model shows slightly higher accuracy and greater efficiency in predicting the FOS.
3. The characteristic parameters of the slopes obtained from indoor experiments were used to establish a finite element model in GeoStudio for FOS analysis. By comparing the FOS predicted by the GBM regression model with the FOS obtained from the finite element model, we find that the difference between the two is small and within an acceptable range of error. The on-site engineering surveys confirmed the presence of cracks on the third step, thus validating the finite element model's prediction that the most critical sliding plane is between the first and sixth steps. Both the numerical results and GBM model predictions are consistent with the actual site conditions.

## References

- [1] Dash, A. K. "Analysis of accidents due to slope failure in Indian opencast coal mines", *Current Science*, 117(2), pp. 304–308, 2019. <https://doi.org/10.18520/cs/v117/i2/304-308>
- [2] Steiakakis, E., Kavouridis, K., Monopolis, D. "Large scale failure of the external waste dump at the "South Field" lignite mine, Northern Greece", *Engineering Geology*, 104(3–4), pp. 269–279, 2009. <https://doi.org/10.1016/j.enggeo.2008.11.008>
- [3] Yang, B. C., Bai, J. X., Duan, Y. T., Wang, Z. P. "The unlocked mechanism and instability prediction of a typical locked-segment-type slope in China: the Chana landslide", *Bulletin of Engineering Geology and the Environment*, 81(12), 493, 2022. <https://doi.org/10.1007/s10064-022-03001-6>
- [4] Xia, Z. G., Motagh, M., Li, T., Roessner, S. "The June 2020 Aniangzhai landslide in Sichuan Province, Southwest China: slope instability analysis from radar and optical satellite remote sensing data", *Landslides*, 19(2), pp. 313–329, 2022. <https://doi.org/10.1007/s10346-021-01777-4>
- [5] Dong, J. H., Qiu, M., Zhao, J. J., Li, H. J., Wu, Q. H. "Deformation instability mechanism of slope in Fa'er Town, Shuicheng County, Guizhou, China", *Alexandria Engineering Journal*, 61(10), pp. 8289–8295, 2022. <https://doi.org/10.1016/j.aej.2022.01.042>
- [6] Li, W., Alves, T. M., Rebesco, M., Sun, J., Li, J., Li, S. Wu, S. "The Baiyun Slide Complex, South China Sea: A modern example of slope instability controlling submarine-channel incision on continental slopes", *Marine and Petroleum Geology*, 114, 104231, 2020. <https://doi.org/10.1016/j.marpetgeo.2020.104231>
- [7] Ray, A., Kumar, R., Bharati, A. K., Rai, R., Singh T. N. "Hazard Chart for Identification of Potential Landslide Due To the Presence of Residual Soil in the Himalayas", *Indian Geotechnical Journal*, 50(4), pp. 604–619, 2020. <https://doi.org/10.1007/s40098-019-00401-6>
- [8] Ray, A., Kumar, V., Kumar, A., Rai, R., Khandelwal, M., Singh, T. N. "Stability prediction of Himalayan residual soil slope using artificial neural network", *Natural Hazards*, 103(3), pp. 3523–3540, 2020. <https://doi.org/10.1007/s11069-020-04141-2>
- [9] Sun, G., Cheng, S., Jiang, W., Zheng, H. "A global procedure for stability analysis of slopes based on the Morgenstern-Price assumption and its applications", *Computers and Geotechnics*, 80, pp. 97–106, 2016. <https://doi.org/10.1016/j.compgeo.2016.06.014>
- [10] Yang, Y., Sun, G., Zheng, H., Yan, C. "An improved numerical manifold method with multiple layers of mathematical cover systems for the stability analysis of soil-rock-mixture slopes", *Engineering Geology*, 264, 105373, 2020. <https://doi.org/10.1016/j.enggeo.2019.105373>
- [11] Zheng, H. "A three-dimensional rigorous method for stability analysis of landslides", *Engineering Geology*, 145–146, pp. 30–40, 2012. <https://doi.org/10.1016/j.enggeo.2012.06.010>
- [12] Yang, Y., Wu, W., Zheng, H. "Investigation of slope stability based on strength-reduction-based numerical manifold method and generalized plastic strain", *International Journal of Rock Mechanics and Mining Sciences*, 164, 105358, 2023. <https://doi.org/10.1016/j.ijrmms.2023.105358>

## Acknowledgements

This research was funded by Key Research and Development Projects of Shaanxi Province (2024QCY-KXJ-176); Department of Transport of Shaanxi Province (22-38K & 23-39R). We thank the anonymous reviewers for their comments on our paper.

## Author contributions

Menghan Zhang: validation, formal analysis, investigation, data curation, writing-original draft preparation, data curation. Jin Wei: Conceptualization, methodology, resources, writing-review and editing, supervision, project administration. All authors have read and agreed to the published version of the manuscript.

## Competing interests

The authors declare that they have no known competing financial interests or personal relationships that could have appeared to influence the work reported in this paper.

- [13] Kang, F., Xu, B., Li, J. J., Zhao, S. Z. "Slope stability evaluation using Gaussian processes with various covariance functions", *Applied Soft Computing*, 60, pp. 387–396, 2017.  
<https://doi.org/10.1016/j.asoc.2017.07.011>
- [14] Griffiths, D. V. "Slope stability analysis by finite elements", *Geotechnique*, 49(3), pp. 387–403, 1999.  
<https://doi.org/10.1680/geot.1999.49.3.387>
- [15] Ouyang, J., Xu, Q. J., Shi, K. B., Yan, X. J., Gong, J. W. "Temperature-driven parameter reduction finite element method for slope stability analysis of earth-rockfill dam", *Yantu Lixue/Rock and Soil Mechanics*, 32(8), pp. 2549–2554, 2011.
- [16] Abdalla, J. A., Attom, M. F., Hawileh R. "Prediction of minimum factor of safety against slope failure in clayey soils using artificial neural network", *Environmental Earth Sciences*, 73(9), pp. 5463–5477, 2015.  
<https://doi.org/10.1007/s12665-014-3800-x>
- [17] Erzin, Y., Cetin, T. "The prediction of the critical factor of safety of homogeneous finite slopes using neural networks and multiple regressions", *Computers & Geosciences*, 51, pp. 305–313, 2013.  
<https://doi.org/10.1016/j.cageo.2012.09.003>
- [18] Flood, I., Kartam, N. "Neural Networks in Civil Engineering. II: Systems and Application", *Journal of Computing in Civil Engineering*, 8(2), pp. 149–162, 1994.  
[https://doi.org/10.1061/\(ASCE\)0887-3801\(1994\)8:2\(149\)](https://doi.org/10.1061/(ASCE)0887-3801(1994)8:2(149))
- [19] Cheng, M. Y., Wu, Y. W., Chen, K. L. "Risk Preference Based Support Vector Machine Inference Model for Slope Collapse Prediction", *Automation in Construction*, 22, pp. 175–181, 2012.  
<https://doi.org/10.1016/j.autcon.2011.06.015>
- [20] Ferentinou, M. D., Sakellariou, M. G. "Computational intelligence tools for the prediction of slope performance", *Computers and Geotechnics*, 34(5), pp. 362–384, 2007.  
<https://doi.org/10.1016/j.compgeo.2007.06.004>
- [21] Wang, H. B., Xu, W. Y., Xu R. C. "Slope stability evaluation using Back Propagation Neural Networks", *Engineering Geology*, 80(3–4), pp. 302–315, 2005.  
<https://doi.org/10.1016/j.enggeo.2005.06.005>
- [22] Kim, J. C., Lee, S. M., Jung, H. S., Lee, S. "Landslide susceptibility mapping using random forest and boosted tree models in Pyeong-Chang, Korea", *Geocarto International*, 33(9), pp. 1000–1015, 2018.  
<https://doi.org/10.1080/10106049.2017.1323964>
- [23] Rahul, Khandelwal, M., Rai, R., Shrivastva, B. K. "Evaluation of dump slope stability of a coal mine using artificial neural network", *Geomechanics and Geophysics for Geo-Energy and Geo-Resources*, 1(3), pp. 69–77, 2015.  
<https://doi.org/10.1007/s40948-015-0009-8>
- [24] Samui, P. "Slope stability analysis: a support vector machine approach", *Environmental Geology*, 56(2), pp. 255–267, 2008.  
<https://doi.org/10.1007/s00254-007-1161-4>
- [25] Zhou, J., Li, E., Yang, S., Wang, M., Shi, X., Yao, S., Mitri, H. S. "Slope stability prediction for circular mode failure using gradient boosting machine approach based on an updated database of case histories", *Safety Science*, 118, pp. 505–518, 2019.  
<https://doi.org/10.1016/j.ssci.2019.05.046>
- [26] Deng, Z. P., Pan, M., Niu, J. T., Jiang, S. H., Qian, W. W. "Slope reliability analysis in spatially variable soils using sliced inverse regressionbased multivariate adaptive regression spline", *Bulletin of Engineering Geology and the Environment*, 80(9), pp. 7213–7226, 2021.  
<https://doi.org/10.1007/s10064-021-02353-9>
- [27] Jiang, S. H., Huang, J., Griffiths, D. V., Deng, Z. P. "Advances in reliability and risk analyses of slopes in spatially variable soils: A state-of-the-art review", *Computers and Geotechnics*, 141, 104498, 2022.  
<https://doi.org/10.1016/j.compgeo.2021.104498>
- [28] Jiang, S. H., Huang, J. S. "Efficient slope reliability analysis at low-probability levels in spatially variable soils", *Computers and Geotechnics*, 75, pp. 18–27, 2016.  
<https://doi.org/10.1016/j.compgeo.2016.01.016>
- [29] Jiang, S. H., Li, D. Q., Zhang, L. M., Zhou, C. B. "Slope reliability analysis considering spatially variable shear strength parameters using a non-intrusive stochastic finite element method", *Engineering Geology*, 168, 120–128, 2014.  
<https://doi.org/10.1016/j.enggeo.2013.11.006>
- [30] Liu, L. L., Cheng, Y. M. "System Reliability Analysis of Soil Slopes Using an Advanced Kriging Metamodel and Quasi-Monte Carlo Simulation", *International Journal of Geomechanics*, 18(8), 06018019, 2018.  
[https://doi.org/10.1061/\(ASCE\)GM.1943-5622.0001209](https://doi.org/10.1061/(ASCE)GM.1943-5622.0001209)
- [31] Wang, L., Wu, C., Gu, X., Liu, H., Zhang, W. "Probabilistic stability analysis of earth dam slope under transient seepage using multivariate adaptive regression splines", *Bulletin of Engineering Geology and the Environment*, 79(6), pp. 2763–2775, 2020.  
<https://doi.org/10.1007/s10064-020-01730-0>
- [32] Wang, L., Wu, C., Tang, L., Zhang, W., Gao, L. "Efficient reliability analysis of earth dam slope stability using extreme gradient boosting method", *Acta Geotechnica*, 15(11), pp. 3135–3150, 2020.  
<https://doi.org/10.1007/s11440-020-00962-4>
- [33] Tien Bui, D., Pradhan, B., Lofman, O., Revhaug, I., Dick, Ø. B. "Regional prediction of landslide hazard using probability analysis of intense rainfall in the Hoa Binh province, Vietnam", *Natural Hazards*, 66(2), pp. 707–730, 2013.  
<https://doi.org/10.1007/s11069-012-0510-0>
- [34] Cheng, M. Y., Hoang, N. D. "Typhoon-induced slope collapse assessment using a novel bee colony optimized support vector classifier", *Natural Hazards*, 78(3), pp. 1961–1978, 2015.  
<https://doi.org/10.1007/s11069-015-1813-8>
- [35] Kang, F., Li, J. "Artificial Bee Colony Algorithm Optimized Support Vector Regression for System Reliability Analysis of Slopes", *Journal of Computing in Civil Engineering*, 30(3), 04015040, 2016.  
[https://doi.org/10.1061/\(ASCE\)CP.1943-5487.0000514](https://doi.org/10.1061/(ASCE)CP.1943-5487.0000514)
- [36] Lu, P., Rosenbaum, M. "Artificial Neural Networks and Grey Systems for the Prediction of Slope Stability", *Natural Hazards*, 30(3), 383–398, 2003.  
<https://doi.org/10.1023/b:nhaz.0000007168.00673.27>
- [37] Dai, F., Lee, C., Deng, J., Tham, L. "The 1786 earthquake-triggered landslide dam and subsequent dam-break flood on the Dadu River, southwestern China", *Geomorphology*, 73(3–4), pp. 277–278, 2005.  
<https://doi.org/10.1016/j.geomorph.2005.06.011>
- [38] Kappes, M. S., Keiler, M., Elverfeldt, K. V., Glade, T. "Challenges of dealing with multi-hazard risk: a review", *Natural Hazards*, 64(2), pp. 1925–1958, 2012.  
<https://doi.org/10.1007/s11069-012-0294-2>